



Published in final edited form as:

Invest Radiol. 2015 May ; 50(5): 322–329. doi:10.1097/RLI.0000000000000128.

Three-dimensional Ultrasound Molecular Imaging of Angiogenesis in Colon Cancer using a Clinical Matrix Array Ultrasound Transducer

Huaijun Wang, MD, PhD¹, Osamu F. Kaneko, MD¹, Lu Tian, PhD², Dimitre Hristov, PhD³, and Jürgen K. Willmann, MD¹

¹Department of Radiology, Molecular Imaging Program at Stanford, Stanford University, School of Medicine, Stanford, California, USA

²Department of Health, Research & Policy, Stanford University, Stanford, California, USA

³Department of Radiation Oncology, Stanford University, Stanford, California, USA

Abstract

Objectives—We sought to assess the feasibility and reproducibility of three-dimensional (3D) ultrasound molecular imaging (USMI) of vascular endothelial growth factor receptor 2 (VEGFR2) expression in tumor angiogenesis using a clinical matrix array transducer and a clinical grade VEGFR2-targeted contrast agent in a murine model of human colon cancer.

Materials and Methods—Animal studies were approved by the Institutional Administrative Panel on Laboratory Animal Care. Mice with human colon cancer xenografts (n=33) were imaged with a clinical ultrasound system and transducer (Philips iU22; X6-1) following intravenous injection of either clinical grade VEGFR2-targeted microbubbles (MB_{VEGFR2}) or non-targeted control microbubbles (MB_{Control}). Nineteen mice were scanned twice to assess imaging reproducibility. Fourteen mice were scanned both before and 24h after treatment with either bevacizumab (n=7) or saline only (n=7). 3D USMI datasets were retrospectively reconstructed into multiple consecutive 1-mm thick USMI data sets to simulate 2D imaging. Vascular VEGFR2 expression was assessed *ex vivo* using immunofluorescence.

Results—3D USMI was highly reproducible using both MB_{VEGFR2} and MB_{Control} (ICC=0.83). VEGFR2-targeted USMI signal significantly ($P=0.02$) decreased by 57% following anti-angiogenic treatment compared to the control group, which correlated well with *ex vivo* VEGFR2 expression on immunofluorescence ($\rho=0.93$, $P=0.003$). If only central 1-mm tumor planes were analyzed to assess anti-angiogenic treatment response, the USMI signal change was significantly ($P=0.006$) overestimated by an average of 27% (range, 2–73%) compared to 3D USMI.

Conclusions—3D USMI is feasible and highly reproducible and allows accurate assessment and monitoring of VEGFR2 expression in tumor angiogenesis in a murine model of human colon cancer.

Corresponding Author: Jürgen K. Willmann, MD, Department of Radiology, Molecular Imaging Program at Stanford, School of Medicine, Stanford University, 300 Pasteur Drive, Room H1307; Stanford, CA 94305-5621, P: 650-723-5424; Fax: 650-723-1909, willmann@stanford.edu.

Conflicts of interest: No.

Keywords

Ultrasound; molecular imaging; three-dimensional; cancer; angiogenesis

INTRODUCTION

Angiogenesis is a well-studied hallmark of cancer (1, 2). Numerous malignancies, including colorectal cancer, secrete angiogenic growth factors that aid in the local growth and metastatic spread of disease (3). Vascular endothelial growth factors (VEGFs) are among the best-studied factors that promote angiogenesis in tumors via binding to various receptors. The interaction with the VEGF receptor 2 (VEGFR2) specifically is key in the signaling cascade that is responsible for endothelial cell proliferation and migration; this ultimately contributes to neovascularization and tumor growth (4, 5).

Several therapies targeted at VEGF, VEGFR, or downstream signaling pathways are being evaluated in multiple clinical trials including in patients with metastatic colorectal cancer (6). Medical imaging plays an important role in evaluating the response of patients undergoing these targeted therapies. Currently, Response Evaluation Criteria in Solid Tumors (RECIST) reporting is used to standardize tumor measurements and determine the responses to therapies in clinical trials. However, many targeted therapies exert cytostatic rather than cytotoxic effects and lead to little change in tumor size despite there being substantial clinical benefit for the patient (7). Therefore, several alternative noninvasive quantitative imaging methods for evaluating treatment response at the molecular level are currently being explored (8–10).

Ultrasound molecular imaging (USMI) using molecularly-targeted contrast microbubbles is one of the emerging imaging modalities for evaluating treatment response to targeted therapies at the molecular level. Some of the inherent advantages of ultrasound include its excellent spatial and temporal resolution, low cost, and wide availability. Moreover, ultrasound can be performed at the bedside in patients with significant comorbidities and the use of microbubbles as contrast agents is safe in patients with renal insufficiency since there are no known nephrotoxic effects (11–14). Microbubbles that target angiogenesis markers such as VEGFR2 allow for the quantification of tumor angiogenesis at the molecular level. Two-dimensional (2D) USMI using microbubbles targeted at VEGFR2 has been introduced to assess anti-angiogenic therapeutic response with high accuracy using immunofluorescence as the reference standard (15–17).

However, heterogeneity in tumor tissue secondary to focal areas of necrosis, hemorrhage or hypoxia can lead to sampling errors with 2D imaging approaches. This becomes particularly problematic when repetitive imaging is required and the transducer must be placed at the exact same position for 2D imaging to allow longitudinal assessment of treatment changes (18–20). Three-dimensional (3D) USMI would have the advantage of measuring expression levels of molecular markers in a more accurate way by including the entire target lesion within the field of view. A recent study using a mechanically stepped transducer has shown that 3D USMI allows more robust molecular marker assessment compared to single plane 2D imaging in a rat fibrosarcoma model (21). However, this approach used a linear motion

stage to mechanically move the transducer over the target region, making it difficult to translate into the clinic (22). The recent introduction of next generation clinical matrix array transducers with micro-beam formers has made 3D USMI of tumor angiogenesis possible without having to mechanically move the transducer, but rather allowing it to be held in a stable position similar to routine ultrasound imaging in the clinic (23).

The purpose of our study was to assess feasibility and reproducibility of 3D USMI of VEGFR2 expression in tumor angiogenesis using a clinical matrix array transducer and a clinical grade VEGFR2-targeted contrast agent in a murine model of human colon cancer.

MATERIALS AND METHODS

Human Colon Cancer Xenografts in Mice

This study was approved by the Institutional Administrative Panel on Laboratory Animal Care. Female nude mice (Charles River; 6–8 weeks old, weighing 20–25 g) were used for the human colon cancer xenograft model. Human LS174T colon adenocarcinoma cells (ATCC, Manassas, VA) were cultured in Minimum Essential Medium supplemented with 10% fetal bovine serum, and grown to 70–80% confluency prior to trypsinization and preparation for injection. 3×10^6 cells were suspended in 50 μ l of Matrigel (BD Biosciences, San Jose, CA), and then injected subcutaneously on the lower hind limb. Tumors were scanned at 7–14 days after tumor cell injection when the tumors had reached 1–2 cm in maximum diameter (mean size, 1.6 cm) by using an electronic caliper available on the ultrasound system.

Clinical Grade VEGFR2-targeted Contrast Microbubbles and Control Microbubbles

Clinical grade VEGFR2-targeted contrast microbubbles (MB_{VEGFR2}; BR55; Bracco Suisse SA, Geneva, Switzerland) were used in this study. These microbubbles contain a mixture of perfluorobutane and nitrogen and are functionalized with lipopeptides consisting of a VEGFR2-binding heterodimeric peptide (5.5-kDa; dissociation constant, $K_D=0.5$ nmol/L) and the phospholipid 1,2-distearoyl-sn-glycerol-3-phosphoethanolamine-N-[amino (polyethylene glycol)-2000] (24–26). The mean number of heterodimeric peptides/mm² of the microbubble shell was $34,200 \pm 1,300$ (range, 31,800–36,600). The mean diameter of MB_{VEGFR2} as assessed by using a cell counter and sizer (Multisizer III Coulter Counter; Beckman Coulter, Fullerton, CA) was 1.5 ± 0.1 μ m (range, 1–3 μ m). Non-targeted microbubbles that lack the VEGFR2-specific lipopeptide were used as control microbubbles (MB_{Control}; Bracco). The binding specificity of MB_{VEGFR2} to murine VEGFR2 was confirmed previously (15).

In Vivo Three-Dimensional Ultrasound Molecular Imaging

Imaging Protocol—All mice were kept anesthetized with 2% isoflurane in room air (administered at 2 L/min) and placed on a heated stage in prone position. Three-dimensional USMI of the tumors was performed using a clinical iU22 ultrasound machine and a clinical xMatrix transducer (x6-1, center frequency, 3.2 MHz, 9212 elements, Philips Medical Systems, Bothel, WA). The of imaging data was acquired with electronical interrogation of a region of interest (ROI) without moving the transducer. The imaging parameters were as

following: voxel dimension, $320 \times 110 \times 210 \mu\text{m}^3$; focal length, 40 mm; mechanical index (MI), 0.05; dynamic range, 40 dB; volume rate, 1 volume/second. All imaging parameters were kept constant for each animal. The transducer was placed in a fixed position using a clamp and coupled to the tumor of the animals using pre-warmed ultrasound gel. To bring the depth of the tumor beyond the near field zone of the clinical transducer, an acoustic standoff of 4 cm was created with ultrasound gel (Figure 1). In all mice, both $\text{MB}_{\text{VEGFR2}}$ and $\text{MB}_{\text{Control}}$ were tested and injected in random order to minimize any bias from the injection order. Via a 27g needle (Vevo Micromarker; VisualSonics, Toronto, Canada) placed in a tail vein, either $5 \times 10^7 \text{MB}_{\text{VEGFR2}}$ (100 μl) or $\text{MB}_{\text{Control}}$ (100 μl) were injected within a 5-second bolus at a constant injection rate by using an infusion pump (Kent Scientific, Torrington, CT). A minimum 30 minutes of waiting time between microbubble injections was observed to allow clearance of microbubbles from previous injections (27–29).

First, B-mode images were acquired to define the anatomy and to delineate the tumor volume. Then, image acquisition was switched to Power Modulation Contrast mode, and $\text{MB}_{\text{VEGFR2}}$ or $\text{MB}_{\text{Control}}$ were injected. After 4 minutes, which allowed the microbubbles to circulate through the tumor volume, imaging was performed for 15 seconds to obtain pre-destruction ultrasound imaging signal, corresponding to the signal from molecularly attached and freely circulating microbubbles (15, 28, 30). Then, a sequence of 5 volumes with high power destructive pulses ($\text{MI}=0.77$) over a 5-second period was applied to destroy all microbubbles in the field of view. Following microbubble destruction, 60 seconds were given to allow microbubbles to recirculate into the tumor volume and imaging datasets post destruction were obtained for 15 seconds corresponding to imaging signal from freely circulating microbubbles. Ultrasound imaging volumes were streamed in real-time using the built-in Digital Navigation Link of the ultrasound machine with custom in-house MevisLab modules written in C++ (31).

Assessment of Reproducibility of Three-Dimensional Ultrasound Molecular Imaging—To test the reproducibility of 3D USMI, in 19 tumor-bearing mice the above mentioned imaging protocol was repeated twice both after $\text{MB}_{\text{VEGFR2}}$ and $\text{MB}_{\text{Control}}$ injections, respectively (Figure 2). The different contrast agent injections were separated by at least 30 minutes waiting time to allow clearance of microbubbles from previous injections (27–29). All mice tolerated the four repetitive injections of contrast agents well.

Monitoring Anti-Angiogenic Treatment Response with Three-Dimensional Ultrasound Molecular Imaging—In an additional group of 14 tumor-bearing mice, the effects of a single dose of anti-angiogenic treatment ($n=7$) with bevacizumab (Avastin, 10 mg/kg i.v.; Genentech, South San Francisco, CA) versus control treatment with i.v. saline only ($n=7$) on the 3D USMI signal was tested (Figure 2). First, mice underwent baseline VEGFR2-targeted scanning at day 0 using the protocol described above. Following treatment with either anti-angiogenic therapy or saline only, 3D USMI was repeated 24 hours later using the same imaging protocol. After scanning at 24 hours, all animals were sacrificed and tumor tissues were harvested for *ex vivo* analysis.

Analysis of Three-Dimensional Ultrasound Molecular Imaging Datasets

All imaging data sets were analyzed in random order by one reader blinded to the microbubble types (MB_{VEGFR2} versus $MB_{Control}$) and to the treatments (anti-angiogenic versus saline treatment). Data processing was performed with an in house custom software developed from MeVisLab (32). In brief, using B-mode imaging data collected prior to contrast agent administration, a volume of interest (VOI) was manually contoured on the 3D B-mode images visualized on axial, sagittal, and coronal planes for each series, covering the entire tumor volume. The software automatically calculated all tumor volumes; the average tumor volume was 2145 mm^3 (range, $524 - 4189 \text{ mm}^3$). The imaging signal of attached microbubbles to VEGFR2 was calculated as the difference of imaging signal intensity (in arbitrary units; a.u.) between pre- and post-destructive linearized imaging signals (15, 33, 34).

To evaluate discrepancies in quantifying treatment effects based on 3D imaging versus imaging in 2D, the acquisition of multiple quasi 2D imaging datasets was simulated by retrospectively segmenting the 3D USMI data sets into multiple consecutive 1-mm thick slices. ROIs were manually drawn over all consecutive 1-mm slices and imaging signal intensity changes before and after anti-angiogenic treatment were measured for each 1-mm slice. To assess the degree to which a single 1-mm slice could misrepresent anti-angiogenic treatment response of tumors compared to 3D imaging of the entire tumor volume, ratios of imaging signals after and before anti-angiogenic treatment obtained from each 1-mm slice were compared to the ratios of imaging signals after and before treatment obtained from 3D imaging, and the percent differences between those ratios were calculated.

Ex Vivo Analysis of Tumors

Before extraction, all tumors were marked on the cranial and caudal edges (elevation direction from head to feet in ultrasound imaging) as well as at the dorsal and left tumor surfaces using dyes with four different colors (Davidson Marking System; Bradley Products, Bloomington, MN). This allowed preservation of the spatial orientation of tumor tissues during tissue fixation and sectioning.

Tumor tissues were fixed in 4% paraformaldehyde overnight at 4°C and then cryopreserved in a 30% sucrose solution. Samples were placed in optimal cutting temperature media (OCT; Tissue-Tek, Sakura Finetek, Torrance, CA), frozen, and then sectioned into multiple 1-mm blocks by using a cryomicrotome to allow approximate alignment with the 1-mm slices reconstructed from the 3D datasets. Out of each 1-mm tissue block, a representative $10 \mu\text{m}$ section from the center of the block was selected for quantification of VEGFR2 expression and percent area of blood vessels (see below).

Expression of VEGFR2 was visualized using standard immunofluorescence procedures. In brief, sections were incubated in phosphate buffered saline (PBS) for 10 min to remove remaining OCT and permeabilized for 10 min in 0.5% Triton-X 100 in PBS. Sections were blocked in a solution containing 3% Bovine Serum Albumin (Sigma, St. Louis, MO), 3% goat serum (Sigma) and 3% donkey serum (Sigma) for 30 min at room temperature prior to incubation with primary antibodies [1:100 rabbit-anti-mouse VEGFR2 (Cell Signaling,

Danvers, MA), and 1:250 rat anti-mouse CD31 (eBioscience, San Jose, CA)]. Primary antibodies were visualized with 1:250 AlexaFluor 546 goat anti-rabbit IgG (Invitrogen, Grand Island, NY) and with 1:250 AlexaFluor488 donkey anti-rat IgG (Invitrogen). Samples were mounted in aqueous mounting media (BiogeneX, San Ramon, Ca), and fluorescent images were acquired using Metamorph software (Universal Imaging Corp., West Chester, PA) and a LSM510 metaconfocal microscope (Zeiss, Maple Grove, MN) attached to a digital camera (AxioCam MRc, Bernried, Germany). Multiple single confocal slices (10 μm) were collected and displayed using a 20X objective. By using ImageJ software (National Institutes of Health, Bethesda, MD), both VEGFR2 expression and the percent area of blood vessels per field of view were quantified as the average value from at least five randomly selected fields of view (single field of view area, 0.19 mm^2) in the different tumor slices. In each field, CD31 was used to identify blood vessels, and the mean fluorescent intensity of VEGFR2 within the region of interest and percent area of blood vessels (guided by CD31 staining) were measured in treated and control tumors. Both the overall mean expression of VEGFR2 and the mean percent area of blood vessels per whole tumor volume were calculated by averaging the respective values obtained from all consecutive slices per tumor.

Statistical Analysis

All continuous measurements were expressed as means \pm standard deviation. To measure the reproducibility of 3D USMI using both $\text{MB}_{\text{VEGFR2}}$ and $\text{MB}_{\text{Control}}$, intraclass correlation coefficients (ICCs) along with 95% confidence intervals (CI) were calculated. ICC of 0–0.20 indicated no agreement; ICC of 0.21–0.40, poor agreement; ICC of 0.41–0.60, moderate agreement; ICC of 0.61–0.80, good agreement; and ICC greater than 0.80, excellent agreement (35). Signal intensities obtained in the same mice using both $\text{MB}_{\text{VEGFR2}}$ and $\text{MB}_{\text{Control}}$ were compared with the paired t-test. Changes in imaging signal using $\text{MB}_{\text{VEGFR2}}$ at 24 hours following either anti-angiogenic or saline only treatment were compared using a two-sample Wilcoxon rank test. To show slice-to-slice variability in simulated 2D imaging, the coefficient of variation was calculated as the ratio between the standard deviation and the mean value of imaging signals from all the 1-mm slices for the same tumor. The Spearman correlation coefficient (ρ) between *in vivo* 3D USMI signals and *ex vivo* VEGFR2 expression levels from the same mice was calculated. All statistical analyses were performed with commercially available software (IBM SPSS statistics software, version 20; IBM Corp., Chicago, Ill., USA). The significance level was set at 0.05.

RESULTS

Reproducibility of Three-Dimensional Ultrasound Molecular Imaging

In tumor-bearing animals undergoing two consecutive injections of both $\text{MB}_{\text{VEGFR2}}$ and $\text{MB}_{\text{Control}}$, respectively, the overall reproducibility of 3D USMI was excellent for both microbubble types (Figure 3).

Using $\text{MB}_{\text{VEGFR2}}$, the average imaging signal in human colon cancer xenografts was $1.11 \times 10^6 \pm 5.70 \times 10^5$ a.u. after the first contrast agent injection. This was not significantly different ($P=0.07$) compared to the average imaging signal after the second injection ($1.28 \times 10^6 \pm 7.66 \times 10^5$ a.u.; ICC = 0.83; 95% CI, 0.62–0.93). Similarly, using $\text{MB}_{\text{Control}}$,

average imaging signal in human colon cancer xenografts was $2.84 \times 10^5 \pm 2.65 \times 10^5$ a.u. after the first contrast agent injection, which was not significantly different ($P=0.28$) compared to the second injection ($3.22 \times 10^5 \pm 2.43 \times 10^5$; ICC=0.83; 95% CI, 0.60–0.93). Imaging signal using MB_{VEGFR2} was significantly higher compared to MB_{Control} ($P < 0.001$).

Monitoring Anti-Angiogenic Treatment Response with Three-Dimensional Ultrasound Molecular Imaging

Tumor volumes were not significantly different ($P=0.65$) before treatment (mean, $1603 \text{ mm}^3 \pm 852$) in the saline only control group versus $1760 \text{ mm}^3 \pm 525$ in the anti-angiogenic treatment group. At 24 hours after treatment, the tumor volume increased by $16 \pm 18\%$ ($P=0.52$) in the control group compared to baseline and by $8 \pm 11\%$ ($P=0.57$) in the treatment group; the tumor volumes in the two animal groups remained not significantly different between both treatment groups ($P=0.14$). In contrast, following a single dose of bevacizumab, 3D USMI signal in human colon cancer xenografts significantly decreased by an average of 57% ($P=0.02$; Figure 4). 3D USMI signal increased by an average of 26% within one day in control animals treated with saline only ($P=0.41$).

Comparison of Ultrasound Molecular Imaging Signal Intensities on Three-dimensional Versus Quasi Two-Dimensional Datasets

Overall, VEGFR2-targeted USMI signal intensities obtained from multiple 1-mm planes reconstructed at 1-mm increments showed substantial spatial heterogeneity within tumors before treatment (coefficient of variation = 0.43; 95% CI, 0.35–0.51). This spatial heterogeneity further increased significantly ($P=0.006$) after anti-angiogenic treatment (coefficient of variation=1.1; 95% CI, 0.45–1.77; Figure 5).

To assess the degree to which a single 1-mm plane could misrepresent anti-angiogenic treatment response of tumors compared to 3D imaging of the entire tumor volume, ratios of imaging signals after and before anti-angiogenic treatment obtained from 1-mm slices were compared to the ratios of imaging signals after and before treatment obtained from 3D imaging, and percent differences between each 2D slice and 3D were plotted in Figure 6. To further evaluate how quantitative assessment of treatment response would change if only the central tumor plane was analyzed, the percent differences in signal intensity changes before and after anti-angiogenic treatment were calculated for each animal for both the 3D and the central 1-mm images. In all tumors, treatment response was significantly overestimated ($P=0.006$) by an average of 27% (range, 2–73%) on central planes versus 3D imaging.

Ex Vivo Analysis of Tumors

Following anti-angiogenic treatment, VEGFR2 expression levels on immunofluorescence in human colon cancer xenografts was significantly ($P=0.03$) smaller (9.9 ± 2.3 a.u.) compared to saline treated tumors (16.8 ± 4.3 a.u.), which correlated well with *in vivo* 3D USMI imaging signal ($\rho=0.93$, $P=0.003$; Figure 4). Similarly, the percent area of blood vessels was significantly ($P=0.03$) decreased in bevacizumab-treated ($1.7 \pm 0.9\%$) compared to saline-treated tumors ($5.9 \pm 3.7\%$). Furthermore, quantitative immunofluorescence analysis of multiple consecutive 1mm tissue blocks showed substantial variance of both VEGFR2

expression (coefficient of variation =0.51; 95% CI, 0.32–0.71) and percent area of blood vessels (coefficient of variation=1.00; 95% CI, 0.1–2.06) across the tumors.

DISCUSSION

Our results suggest that 3D USMI using a clinical ultrasound system and a clinical grade VEGFR2-targeted contrast agent is both feasible and highly reproducible and allows for the assessment of anti-angiogenic treatment response in a human colon cancer xenograft model. In addition, our results show spatial heterogeneity of VEGFR2 expression in tumors, suggesting that 3D USMI may be more robust for assessing tumor angiogenesis than traditional 2D USMI.

Human solid tumors are biologically heterogeneous on both genetic and histopathological levels, which is reflected by the spatial variations in cellular density, angiogenesis, and microenvironmental components (36, 37). Regarding angiogenesis, it has been shown that VEGF expression is heterogeneously distributed within solid tumors and undergoes dynamic change during tumor growth (38). Being able to account for this heterogeneity is critical in characterizing malignancies, predicting the clinical outcomes of anti-angiogenic therapies, and assessing therapeutic responses (39, 40). Various imaging modalities are being explored to noninvasively assess angiogenesis, including MRI (39, 40), CT (41–43), PET (44), and ultrasound (21). Ultrasound is advantageous due to its relatively low cost, wide availability, and the lack of radiation exposure, which allows multiple repetitive exams that may be helpful in the future design of more individualized treatment regimens. While 2D USMI has been shown to be an effective tool for imaging and monitoring angiogenesis (15–17), a potential drawback is the difficulty of assessing the spatial and temporal intra-tumoral angiogenesis heterogeneity due to the limitation of imaging only one arbitrary plane. This problem is compounded when longitudinally assessing changes in tumor neovascularity. Therefore, the assessment of tumor angiogenesis along the entire 3D volume in cancer is critically important for USMI if it is to be further developed for monitoring treatment response in patients.

Recently, the feasibility of 3D USMI has been explored in eight subcutaneous rat fibrosarcoma tumors imaged with an $\alpha_v\beta_3$ integrin-targeted contrast agent (21). In that study, a linear array 15L8 transducer was mechanically stepped elevationally in 800 micrometer increments over the tumor volume and multiple 2D data were merged into a single 3D USMI dataset. In our study, we explored whether 3D USMI can be further refined to reproducibly assess tumor angiogenesis by using a clinical matrix array transducer. This transducer allows quantification of molecular marker expression levels over an entire tumor volume at a fixed position without the need for mechanically moving the transducer over the tumor. Nineteen tumors were imaged twice both with molecularly-targeted and non-targeted contrast agents. Our results showed that 3D USMI was highly reproducible for both contrast agent types with an ICC value of 0.83 each. Also, 3D USMI signal intensities using VEGFR2-targeted microbubbles was substantially higher compared to non-targeted microbubbles, confirming target specificity of the clinical grade VEGFR2-targeted contrast agent used in our study, as shown previously by 2D USMI in various animal models (15, 26, 45–48).

We then tested 3D USMI for *in vivo* monitoring of tumor angiogenesis during anti-angiogenic treatment with bevacizumab in a clinically relevant human colon cancer xenograft model. Bevacizumab is a recombinant humanized monoclonal IgG1 antibody that comprise of human framework regions (~93% human and 7% murine protein sequence) (49) which has been shown to be effective in human cancer xenograft models in mice (50), and which is currently used in patients with colorectal cancer, as well as various other cancer types (51–54). *In vivo* 3D USMI signal substantially decreased as early as 24 hours after a single dose of bevacizumab. In contrast, 3D USMI remained substantially higher in control mice receiving saline only. Notably, tumor sizes were not significantly different in treated versus non-treated mice within 24 hours, suggesting that 3D USMI allows early anti-angiogenic treatment effect assessment before overt morphologic-anatomic changes of the tumor become visible. This was further corroborated by quantitative immunofluorescence used as reference standard confirming decreased VEGFR2 expression levels along with decreased percent area of blood vessels in treated tumors.

We further assessed the effects of 3D USMI compared to simulated 2D USMI in terms of assessing quantitative changes in USMI signal intensities following anti-angiogenic therapy. For this purpose, the 3D USMI datasets of each tumor were retrospectively reconstructed into multiple 1-mm slices in 1-mm increments. Our data showed substantial slice-to-slice variability of USMI signals, at both baseline and even more pronounced after anti-angiogenic treatment. More importantly, treatment effects were substantially over- or underestimated when single 2D slices were analyzed compared to 3D USMI. Variability between 2D and 3D USMI in terms of assessment of treatment effects was smaller for the central 2D planes representing the largest tumor diameter, which is usually chosen for 2D ultrasound imaging to represent the entire tumor volume (34, 45). However, treatment response was still overestimated by on average 27% on the central plane compared to 3D USMI, which would make assessment of subtle differences in treatment response in patients difficult. Since histopathologic proof of treatment response as the ultimate reference standard is invasive, expensive, practically challenging, and often not representative for the entire tumor because only a small portion of the tumor is being biopsied (55), 3D USMI may become a promising new surrogate endpoint for assessing treatment response in cancer patients.

We acknowledge several limitations of our study. First, in this proof-of-principle study, only early effects of anti-angiogenic treatment on 3D USMI were assessed at 24 hours. Future studies are warranted to assess its value for monitoring treatment response in cancer over a longer period of time as well as to evaluate the prognostic value of early molecular imaging changes in terms of survival outcomes. Second, we did not obtain 3D US perfusion data in the same animals along with 3D USMI datasets to assess how molecular imaging compares with functional imaging as a quantitative surrogate marker for anti-angiogenic treatment response assessment in cancer. Future studies are warranted comparing both functional and molecular imaging in the same tumors in intra-animal comparison experiments.

In conclusion, our results suggest that 3D USMI using a clinical ultrasound system and matrix array transducer is technically feasible and highly reproducible for assessing tumor angiogenesis in a human colon cancer xenograft model in mice. In addition, 3D USMI using

a clinical grade VEGFR2-targeted contrast agent, which has entered clinical trials most recently (56), allows non-invasive quantification of anti-angiogenic therapeutic effects and may better account for heterogeneity of tumor angiogenesis compared to traditional 2D USMI. The introduction of 3D imaging capabilities on clinical ultrasound systems may further stimulate the future use of USMI in the clinic for objective and reliable monitoring of molecularly-targeted treatment effects.

Acknowledgements

We would like to acknowledge Francois Tranquart, MD PhD (Bracco Suisse SA, Geneva, Switzerland) for providing clinical grade VEGFR2-targeted contrast microbubbles. We also acknowledge Vijay Shandasani, PhD (Philips Healthcare, Bothell, Washington, USA) for providing the clinical ultrasound system and transducer.

Funding support: This research was supported in part by R01 CA155289-01A1 (JKW), R01DK092509-01A1 (JKW), and the Developmental Cancer Research Award from the Stanford Cancer Center Grant (JKW). Huaijun Wang was supported by the Stanford Dean Fellowship award.

REFERENCES

1. Sadanandam A, Lyssiotis CA, Homicsko K, et al. A colorectal cancer classification system that associates cellular phenotype and responses to therapy. *Nat Med.* 2013; 19:619–625. [PubMed: 23584089]
2. Folkman J. Tumor angiogenesis and tissue factor. *Nat Med.* 1996; 2:167–168. [PubMed: 8574960]
3. Takahashi Y, Kitadai Y, Bucana CD, et al. Expression of vascular endothelial growth factor and its receptor, KDR, correlates with vascularity, metastasis, and proliferation of human colon cancer. *Cancer Res.* 1995; 55:3964–3968. [PubMed: 7664263]
4. Fujii H, Matkar P, Liao C, et al. Optimization of Ultrasound-mediated Anti-angiogenic Cancer Gene Therapy. *Mol Ther Nucleic Acids.* 2013; 2:e94. [PubMed: 23695537]
5. Giatromanolaki A, Koukourakis MI, Sivridis E, et al. Activated VEGFR2/KDR pathway in tumour cells and tumour associated vessels of colorectal cancer. *Eur J Clin Invest.* 2007; 37:878–886. [PubMed: 17883421]
6. Grothey A, Van Cutsem E, Sobrero A, et al. Regorafenib monotherapy for previously treated metastatic colorectal cancer (CORRECT): an international, multicentre, randomised, placebo-controlled, phase 3 trial. *Lancet.* 2013; 381:303–312. [PubMed: 23177514]
7. Eisenhauer EA, Therasse P, Bogaerts J, et al. New response evaluation criteria in solid tumours: revised RECIST guideline (version 1.1). *Eur J Cancer.* 2009; 45:228–247. [PubMed: 19097774]
8. Skougaard K, Nielsen D, Jensen BV, Hendel HW. Comparison of EORTC criteria and PERCIST for PET/CT response evaluation of patients with metastatic colorectal cancer treated with irinotecan and cetuximab. *J Nucl Med.* 2013; 54:1026–1031. [PubMed: 23572497]
9. Guimaraes AR, Ross R, Figuereido JL, et al. MRI with magnetic nanoparticles monitors downstream anti-angiogenic effects of mTOR inhibition. *Mol Imaging Biol.* 2011; 13:314–320. [PubMed: 20559742]
10. Weber WA. Assessing tumor response to therapy. *J Nucl Med.* 2009; 50(Suppl 1):1S–10S. [PubMed: 19380403]
11. Coleman JL, Navid F, Furman WL, McCarville MB. Safety of ultrasound contrast agents in the pediatric oncologic population: a single-institution experience. *AJR Am J Roentgenol.* 2014; 202:966–970. [PubMed: 24758648]
12. Correas JM, Bridal L, Lesavre A, et al. Ultrasound contrast agents: properties, principles of action, tolerance, and artifacts. *Eur Radiol.* 2001; 11:1316–1328. [PubMed: 11519538]
13. Jakobsen JA, Oyen R, Thomsen HS, et al. Safety of ultrasound contrast agents. *Eur Radiol.* 2005; 15:941–945. [PubMed: 15662495]

14. Piscaglia F, Bolondi L. Italian Society for Ultrasound in M, Biology Study Group on Ultrasound Contrast A. The safety of Sonovue in abdominal applications: retrospective analysis of 23188 investigations. *Ultrasound Med Biol*. 2006; 32:1369–1375. [PubMed: 16965977]
15. Pysz MA, Foygel K, Rosenberg J, et al. Antiangiogenic cancer therapy: monitoring with molecular US and a clinically translatable contrast agent (BR55). *Radiology*. 2010; 256:519–527. [PubMed: 20515975]
16. Anderson CR, Rychak JJ, Backer M, et al. scVEGF microbubble ultrasound contrast agents: a novel probe for ultrasound molecular imaging of tumor angiogenesis. *Invest Radiol*. 2010; 45:579–585. [PubMed: 20733505]
17. Sirsi SR, Flexman ML, Vlachos F, et al. Contrast ultrasound imaging for identification of early responder tumor models to anti-angiogenic therapy. *Ultrasound Med Biol*. 2012; 38:1019–1029. [PubMed: 22425376]
18. Feingold S, Gessner R, Guracar IM, Dayton PA. Quantitative volumetric perfusion mapping of the microvasculature using contrast ultrasound. *Invest Radiol*. 2010; 45:669–674. [PubMed: 20808232]
19. Zhou JH, Cao LH, Zheng W, et al. Contrast-enhanced gray-scale ultrasound for quantitative evaluation of tumor response to chemotherapy: preliminary results with a mouse hepatoma model. *AJR Am J Roentgenol*. 2011; 196:W13–W17. [PubMed: 21178025]
20. Hoyt K, Sorace A, Saini R. Quantitative mapping of tumor vascularity using volumetric contrast-enhanced ultrasound. *Invest Radiol*. 2012; 47:167–174. [PubMed: 22104962]
21. Streeter JE, Gessner RC, Tsuruta J, et al. Assessment of molecular imaging of angiogenesis with three-dimensional ultrasonography. *Mol Imaging*. 2011; 10:460–468. [PubMed: 22201537]
22. Hu X, Caskey CF, Mahakian LM, et al. In vivo validation and 3D visualization of broadband ultrasound molecular imaging. *Am J Nucl Med Mol Imaging*. 2013; 3:336–349. [PubMed: 23901359]
23. Li QY, Tang J, He EH, et al. Clinical utility of three-dimensional contrast-enhanced ultrasound in the differentiation between noninvasive and invasive neoplasms of urinary bladder. *Eur J Radiol*. 2012; 81:2936–2942. [PubMed: 22260895]
24. Pillai R, Marinelli ER, Swenson RE. A flexible method for preparation of peptide homo- and heterodimers functionalized with affinity probes, chelating ligands, and latent conjugating groups. *Biopolymers*. 2006; 84:576–585. [PubMed: 16845666]
25. Shrivastava A, von Wronski MA, Sato AK, et al. A distinct strategy to generate high-affinity peptide binders to receptor tyrosine kinases. *Protein Eng Des Sel*. 2005; 18:417–424. [PubMed: 16087652]
26. Pochon S, Tardy I, Bussat P, et al. BR55: a lipopeptide-based VEGFR2-targeted ultrasound contrast agent for molecular imaging of angiogenesis. *Invest Radiol*. 2010; 45:89–95. [PubMed: 20027118]
27. Pysz MA, Foygel K, Panje CM, et al. Assessment and monitoring tumor vascularity with contrast-enhanced ultrasound maximum intensity persistence imaging. *Invest Radiol*. 2011; 46:187–195. [PubMed: 21150790]
28. Willmann JK, Cheng Z, Davis C, et al. Targeted microbubbles for imaging tumor angiogenesis: assessment of whole-body biodistribution with dynamic micro-PET in mice. *Radiology*. 2008; 249:212–219. [PubMed: 18695212]
29. Palmowski M, Morgenstern B, Hauff P, et al. Pharmacodynamics of streptavidin-coated cyanoacrylate microbubbles designed for molecular ultrasound imaging. *Invest Radiol*. 2008; 43:162–169. [PubMed: 18301312]
30. Deshpande N, Ren Y, Foygel K, et al. Tumor angiogenic marker expression levels during tumor growth: longitudinal assessment with molecularly targeted microbubbles and US imaging. *Radiology*. 2011; 258:804–811. [PubMed: 21339349]
31. Schlosser J, Kirmizibayrak C, Shamdasani V, et al. Automatic 3D ultrasound calibration for image guided therapy using intramodality image registration. *Phys Med Biol*. 2013; 58:7481–7496. [PubMed: 24099806]

32. Heckel F, Schwier M, H-O P. Object Oriented Application Development with MeVisLab and Python. *Lecture Notes in Informatics (Informatik 2009: Im Focus das Leben)*. 2009; 154:1338–1351.
33. Sorace AG, Saini R, Mahoney M, Hoyt K. Molecular ultrasound imaging using a targeted contrast agent for assessing early tumor response to antiangiogenic therapy. *J Ultrasound Med*. 2012; 31:1543–1550. [PubMed: 23011617]
34. Wei S, Fu N, Sun Y, et al. Targeted Contrast-Enhanced Ultrasound Imaging of Angiogenesis in an Orthotopic Mouse Tumor Model of Renal Carcinoma. *Ultrasound Med Biol*. 2014; 40:1250–1259. [PubMed: 24613557]
35. Faria JR, Araao AR, Jimenez LM, et al. Inter-rater concordance study of the PASI (Psoriasis Area and Severity Index). *An Bras Dermatol*. 2010; 85:625–629. [PubMed: 21152786]
36. Marusyk A, Almendro V, Polyak K. Intra-tumour heterogeneity: a looking glass for cancer? *Nat Rev Cancer*. 2012; 12:323–334. [PubMed: 22513401]
37. Davnall F, Yip CS, Ljungqvist G, et al. Assessment of tumor heterogeneity: an emerging imaging tool for clinical practice? *Insights Imaging*. 2012; 3:573–589. [PubMed: 23093486]
38. Kumar R, Kuniyasu H, Bucana CD, et al. Spatial and temporal expression of angiogenic molecules during tumor growth and progression. *Oncol Res*. 1998; 10:301–311. [PubMed: 9848101]
39. O'Connor JP, Rose CJ, Jackson A, et al. DCE-MRI biomarkers of tumour heterogeneity predict CRC liver metastasis shrinkage following bevacizumab and FOLFOX-6. *Br J Cancer*. 2011; 105:139–145. [PubMed: 21673686]
40. Zhu W, Kato Y, Artemov D. Heterogeneity of tumor vasculature and antiangiogenic intervention: insights from MR angiography and DCE-MRI. *PLoS One*. 2014; 9:e86583. [PubMed: 24466160]
41. Sanghera B, Banerjee D, Khan A, et al. Reproducibility of 2D and 3D fractal analysis techniques for the assessment of spatial heterogeneity of regional blood flow in rectal cancer. *Radiology*. 2012; 263:865–873. [PubMed: 22438361]
42. Ren Y, Fleischmann D, Foygel K, et al. Antiangiogenic and radiation therapy: early effects on in vivo computed tomography perfusion parameters in human colon cancer xenografts in mice. *Invest Radiol*. 2012; 47:25–32. [PubMed: 22178893]
43. Poschinger T, Renner A, Eisa F, et al. Dynamic Contrast-Enhanced Micro-Computed Tomography Correlates With 3-Dimensional Fluorescence Ultramicroscopy in Antiangiogenic Therapy of Breast Cancer Xenografts. *Invest Radiol*. 2014; 49:445–456. [PubMed: 24598441]
44. Nagengast WB, Lub-de Hooge MN, Oosting SF, et al. VEGF-PET imaging is a noninvasive biomarker showing differential changes in the tumor during sunitinib treatment. *Cancer Res*. 2011; 71:143–153. [PubMed: 21084271]
45. Frinking PJ, Tardy I, Theraulaz M, et al. Effects of acoustic radiation force on the binding efficiency of BR55, a VEGFR2-specific ultrasound contrast agent. *Ultrasound Med Biol*. 2012; 38:1460–1469. [PubMed: 22579540]
46. Bachawal SV, Jensen KC, Lutz AM, et al. Earlier detection of breast cancer with ultrasound molecular imaging in a transgenic mouse model. *Cancer Res*. 2013; 73:1689–1698. [PubMed: 23328585]
47. Bzyl J, Palmowski M, Rix A, et al. The high angiogenic activity in very early breast cancer enables reliable imaging with VEGFR2-targeted microbubbles (BR55). *European Radiology*. 2013; 23:468–475. [PubMed: 22878592]
48. Pysz MA, Machtaler SB, Seeley ES, et al. Vascular Endothelial Growth Factor Receptor Type 2-targeted Contrast-enhanced US of Pancreatic Cancer Neovasculature in a Genetically Engineered Mouse Model: Potential for Earlier Detection. *Radiology*. 2014 Epub. DOI: <http://dx.doi.org/10.1148/radiol.14140568>.
49. Gerber HP, Ferrara N. Pharmacology and pharmacodynamics of bevacizumab as monotherapy or in combination with cytotoxic therapy in preclinical studies. *Cancer Res*. 2005; 65:671–680. [PubMed: 15705858]
50. Paudyal B, Paudyal P, Shah D, et al. Detection of vascular endothelial growth factor in colon cancer xenografts using bevacizumab based near infrared fluorophore conjugate. *J Biomed Sci*. 2014; 21:35. [PubMed: 24780003]

51. Tie J, Desai J. Antiangiogenic therapies targeting the vascular endothelia growth factor signaling system. *Crit Rev Oncog*. 2012; 17:51–67. [PubMed: 22471664]
52. Bennouna J, Sastre J, Arnold D, et al. Continuation of bevacizumab after first progression in metastatic colorectal cancer (ML18147): a randomised phase 3 trial. *Lancet Oncol*. 2013; 14:29–37. [PubMed: 23168366]
53. Ciombor KK, Berlin J. Targeting metastatic colorectal cancer - present and emerging treatment options. *Pharmgenomics Pers Med*. 2014; 7:137–144. [PubMed: 25045279]
54. Lee JJ, Chu E. Sequencing of Antiangiogenic Agents in the Treatment of Metastatic Colorectal Cancer. *Clin Colorectal Cancer*. 2014; 13:135–144. [PubMed: 24768040]
55. Bedard PL, Hansen AR, Ratain MJ, Siu LL. Tumour heterogeneity in the clinic. *Nature*. 2013; 501:355–364. [PubMed: 24048068]
56. Kaneko OF, Willmann JK. Ultrasound for molecular imaging and therapy in cancer. *Quant Imaging Med Surg*. 2012; 2:87–97. [PubMed: 23061039]

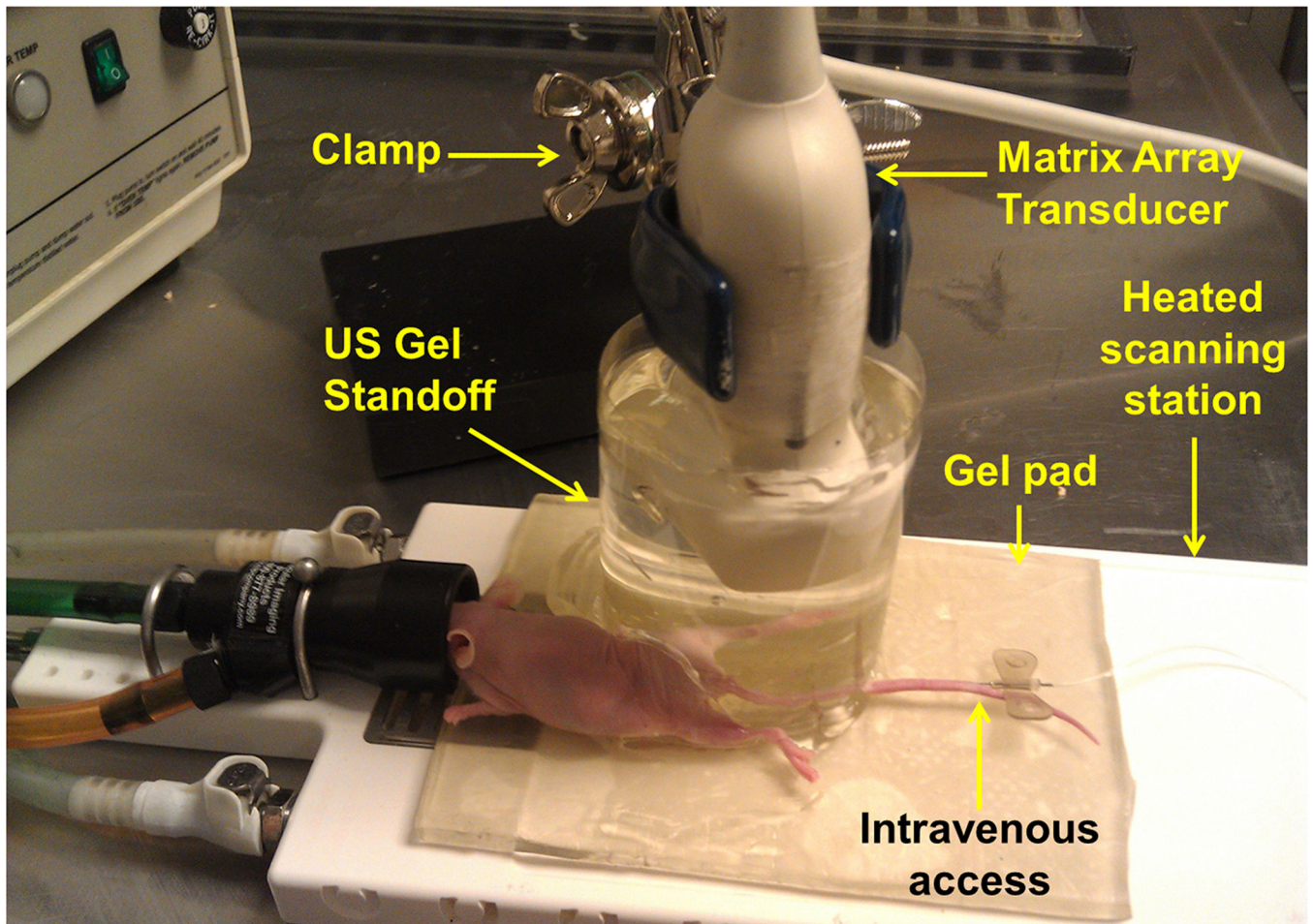


Figure 1. Photograph of the imaging setting for three-dimensional (3D) ultrasound molecular imaging (USMI) using a clinical matrix array transducer in mice. To bring the subcutaneous human colon cancer xenograft implanted on the hind limb beyond the near field zone of the transducer, the transducer was embedded in a custom standoff, which was comprised of a column of pre-warmed ultrasound gel contained within a plastic cylindrical chamber. All mice were kept under inhalation anesthesia during scanning and body temperature was kept constant by placing them on a gel pad on a heated scanning station. Note, a needle was placed in one of the two tail veins to allow intravenous administration of contrast microbubbles.

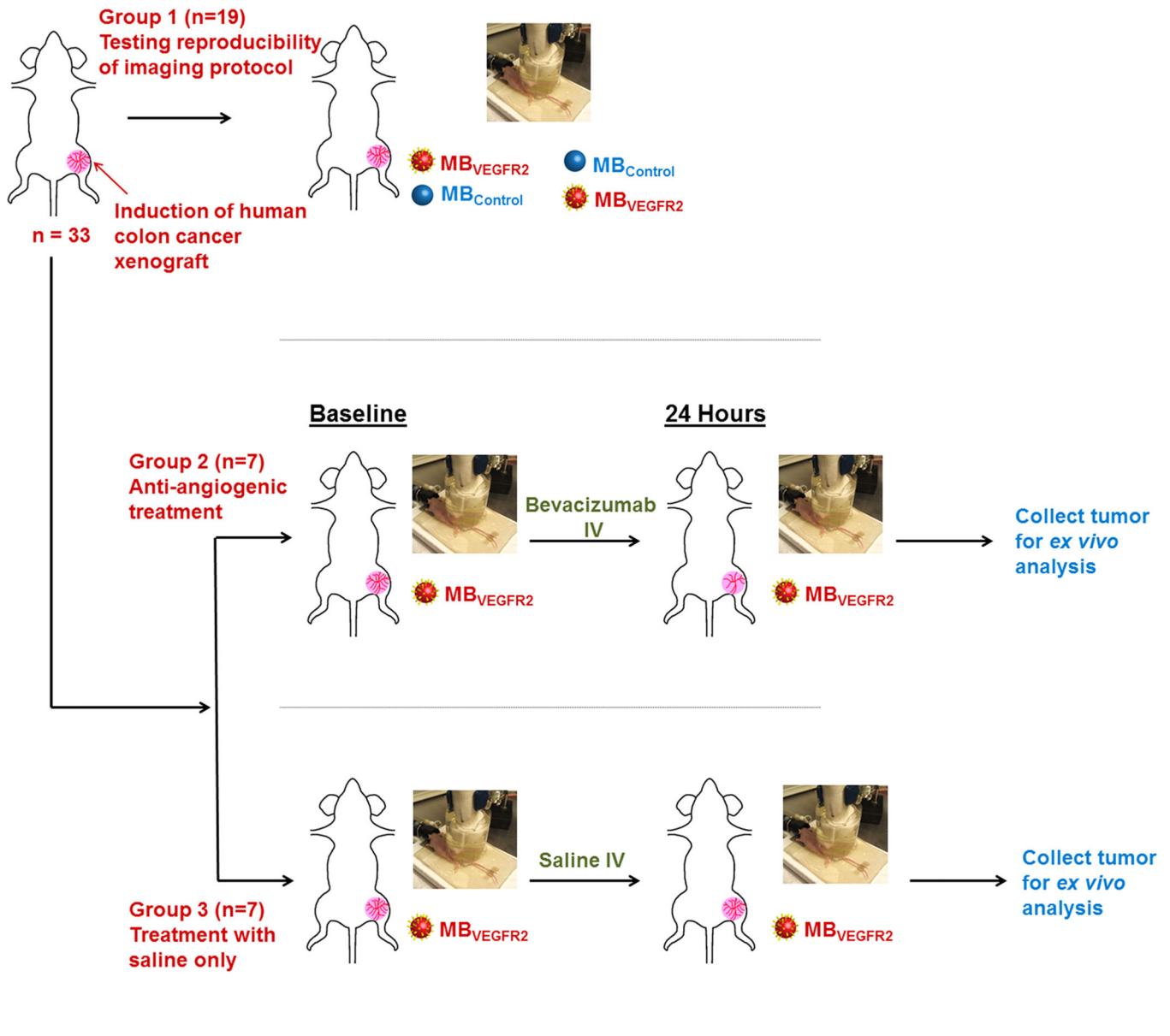


Figure 2.

Overview of experimental design. In 33 nude mice, subcutaneous human colon cancer xenografts were randomized into three groups. In group 1 (n=19), two consecutive 3D USMI exams using MB_{VEGFR2} and $MB_{Control}$ each in random order in the same imaging session were performed to assess reproducibility of the imaging technique (total of 4 injections). Mice in group 2 (n=7) were scanned before and 24 hours after a single dose of bevacizumab; mice in group 3 (n=7) served as control group without anti-angiogenic treatment. After scanning, tumor tissues were harvested for *ex vivo* analysis.

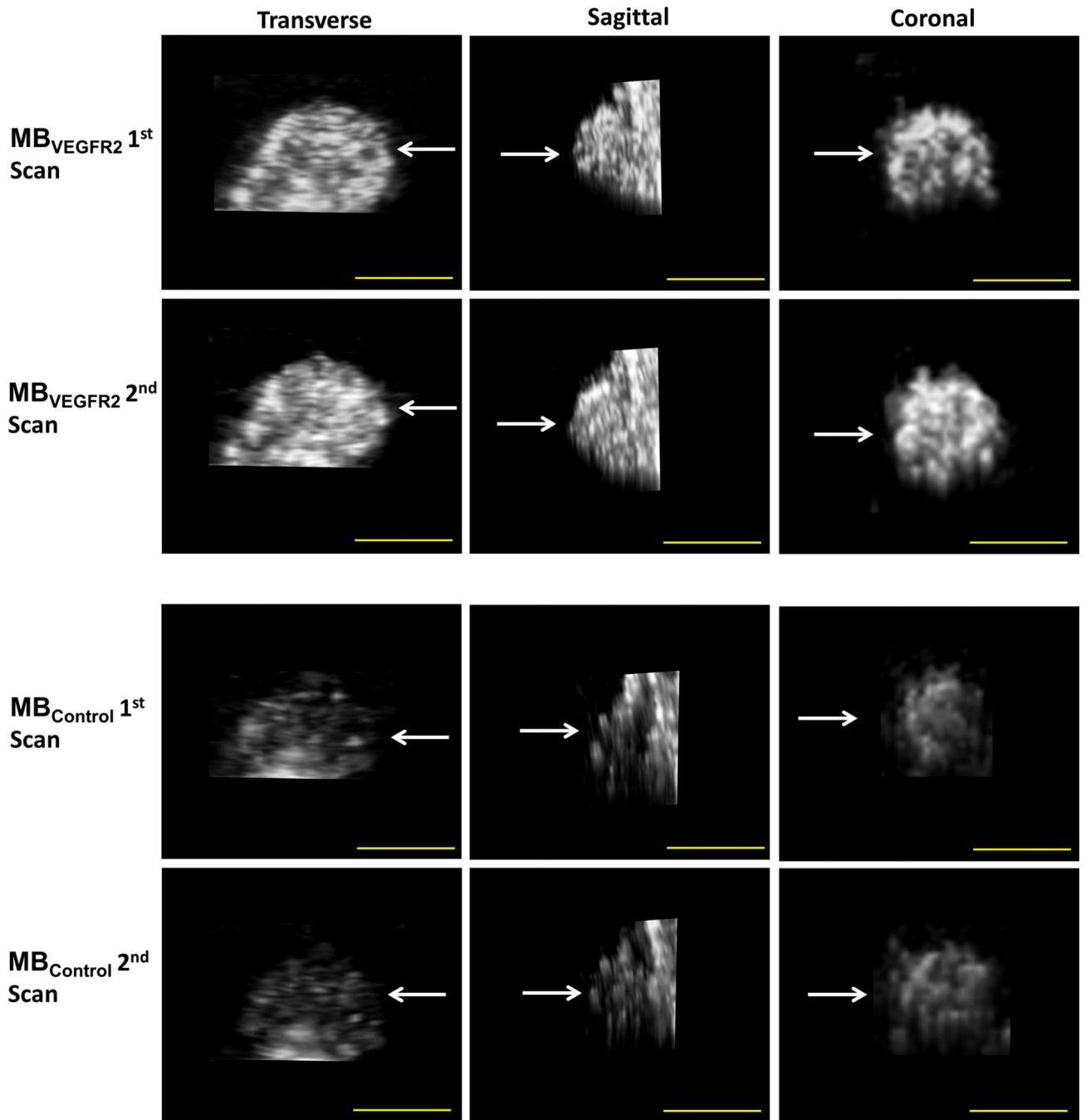


Figure 3. Representative subcutaneous human colon cancer xenograft imaged twice with both MB_{VEGFR2} and $MB_{Control}$. Transverse, sagittal, and coronal views through the center of the tumor (arrows) are shown. Note, similar signal distribution on repeated scans using both contrast agent types as well as substantially higher imaging signal using MB_{VEGFR2} compared to $MB_{Control}$ in the same tumor. Scale bar = 10 mm.

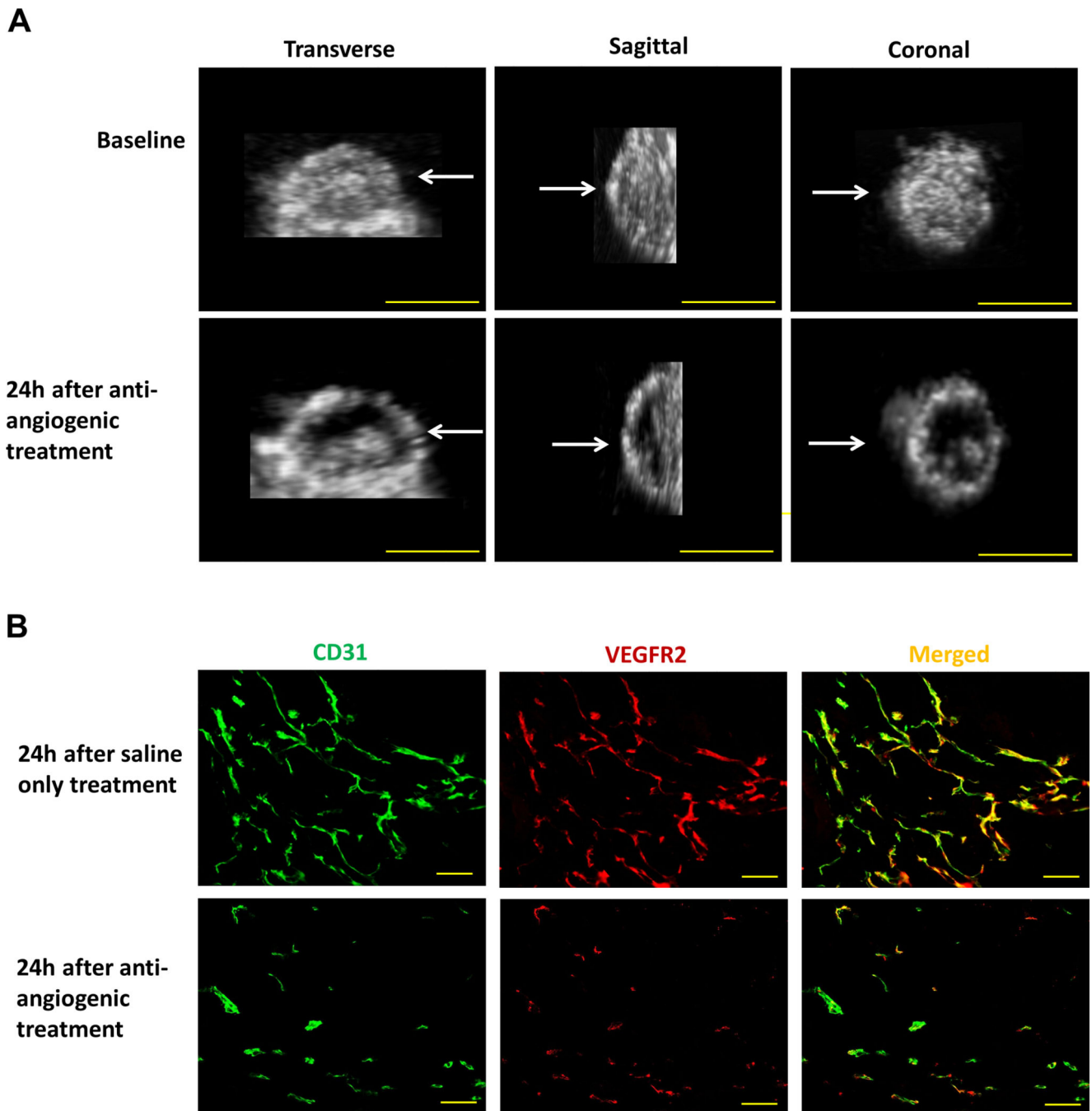


Figure 4.

(A) The effect of anti-angiogenic treatment on VEGFR2-targeted 3D USMI signal in representative subcutaneous human colon cancer xenograft. 3D USMI signal, as visualized on transverse, sagittal, and coronal views, substantially decreased 24 hours after administration of bevacizumab (lower row) compared to baseline imaging (upper row); scale bar = 10 mm. (B) Photomicrograph of merged (yellow) VEGFR2 (red) and CD31 (green) stained tissue slices obtained from the tumor center in the same mouse confirmed treatment

effect with both decreased VEGFR2 expression levels and percent area of blood vessels in bevacizumab-treated versus saline-treated tumor; scale bar = 100 μ m.

Author Manuscript

Author Manuscript

Author Manuscript

Author Manuscript

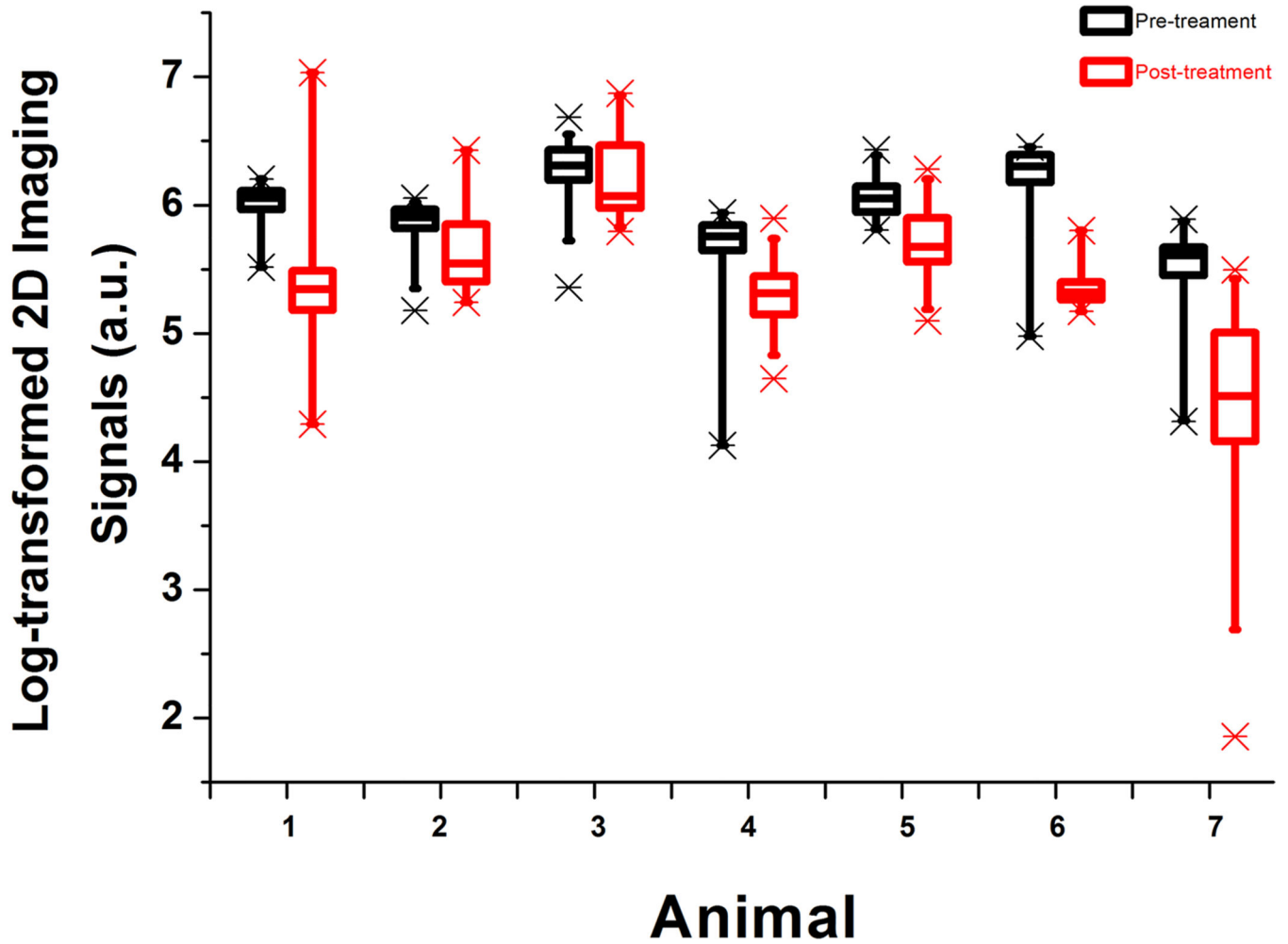


Figure 5.

Spatial heterogeneity of tumor angiogenesis demonstrated for all seven subcutaneous human colon cancer xenografts imaged with VEGFR2-targeted USMI before (black box plots) and 24 hours after (red box plots) anti-angiogenic therapy with bevacizumab. 3D datasets were retrospectively segmented into different numbers (depending on tumor size) of consecutive 1-mm datasets and logarithmically transformed imaging signals were then plotted for each animal separately. Each box in the plot represents the 25th and 75th quartiles, the line inside each box identifies the median and the whiskers indicate the 5th and 95th percentile of measurements excluding the outliers. Asterisks represent outliers. Note substantial ranges of USMI signal intensities among consecutive 1-mm planes both before and after anti-angiogenic therapy.

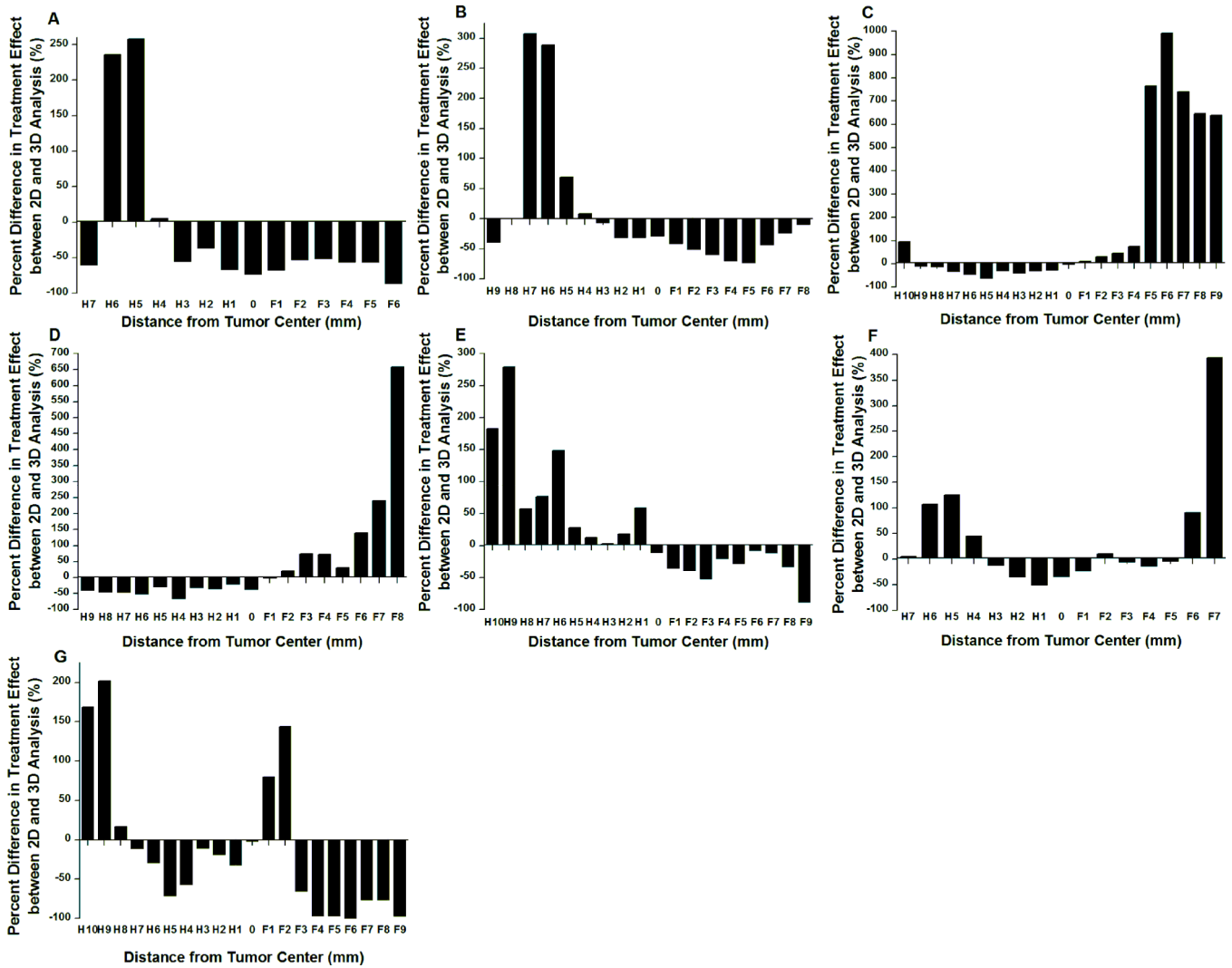


Figure 6. Bar charts show differences in anti-angiogenic treatment effects based on data analysis of various 1-mm planes versus 3D USMI images for each of the seven tumors treated with anti-angiogenic therapy (A–G). Ratios of imaging signals after and before anti-angiogenic treatment obtained from 1-mm planes were compared to the ratios of imaging signals after and before treatment obtained from 3D imaging, and percent differences were plotted. Note that treatment response can be either over-estimated or under-estimated compared to 3D imaging. H: head (cranial part of the tumor); F: foot (caudal part of the tumor). 0: Center of the tumor. Each 1-mm plane was numbered consecutively compared to the center of the tumor in 1 mm increments.